ChemPubSoc Europe

DOI: 10.1002/ejic.201601450

EurJIC European Journal of Inorganic Chemistry

Full Paper

Photochemical Anticancer Complexes | *Very Important Paper* |

CLUSTER ISSUE

VIP

Photochemical Properties and Structure–Activity Relationships of Ru^{II} Complexes with Pyridylbenzazole Ligands as Promising Anticancer Agents

Dmytro Havrylyuk,[a] David K. Heidary,[a] Leona Nease,[a] Sean Parkin,[a] and Edith C. Glazer*[a]

Abstract: Ruthenium complexes capable of light-triggered cytotoxicity are appealing potential prodrugs for photodynamic therapy (PDT) and photoactivated chemotherapy (PACT). Two groups of (polypyridyl)Ru^{II} complexes with 2-(2-pyridyl)benzazole ligands were synthesized and investigated for their photochemical properties and anticancer activity to compare strained and unstrained systems that are likely to have different biological mechanisms of action. The structure–activity relationship was focused on the benzazole-core bioisosterism and replacement of coligands in Ru^{II} complexes. Strained compounds rapidly ejected the 2-(2-pyridyl)benzazole ligand after light irradiation, and possessed strong toxicity in the HL-60 cell line both under dark and light conditions. In contrast, unstrained Ru^{II} complexes were nontoxic in the absence of light, induced cytotoxicity at nanomolar concentrations after light irradiation, and were capable of light-induced DNA damage. The 90–220-fold difference in light and dark IC_{50} values provides a large potential therapeutic window to allow for selective targeting of cells by exposure to light.

Introduction

Cancer is currently the second leading cause of death in the United States, following heart disease. More than 1.7 million people are estimated to have been diagnosed with cancer in 2016.[1] With global cancer morbidity rising, the development of new cancer treatments is crucial. Chemotherapy is used in most treatment regimens for cancer. Since its discovery in the late 1960s, cisplatin and derivatives thereof have achieved great success, and nearly 50 % of patients being treated for cancer are given a platinum-based drug.[2] Widespread treatment with cisplatin, however, has revealed major clinical problems associated with its use. Cisplatin has dose-limiting side-effects, such as nephrotoxicity, neurotoxicity, ototoxicity, and myelosuppression.[3] Due to these severe side-effects, cisplatin has to be administered at concentrations that might not be lethal to tumor cells, thereby facilitating development of drug resistance. These limitations have driven the investigations of other (non-platinum) transition-metal compounds.

In recent years, ruthenium-based complexes have emerged as promising antitumor and antimetastatic agents, with potential uses in platinum-resistant tumors.[4] Ruthenium compounds are well suited for medical applications, due to a combination of chemical and biological properties: they can form multiple geometries with facile ligand exchange, they can be activated by environmental features or external triggers, and they are capable of mimicking iron binding for transportation.[5] The different oxidation states can be exploited to design prodrugs, where the inactive 3+ ruthenium complexes can be reduced to 2+, creating an active species and a biological effect. The reducing environment of tumors has been associated with the selective activity of ruthenium-based drugs NAMI-A, KP1019, and KP1339, which have been investigated in clinical trials.[6] An alternative prodrug strategy is to use light to transform inert complexes into cytotoxic agents.[7] We have demonstrated that this can be accomplished with strained (polypyridyl)Ru^{II} complexes with distorted octahedral geometry, which photo-decompose by ligand dissociation.[8] The resulting ligand-deficient Ru^{II} center can covalently modify DNA or other biomolecules, and induce cytotoxicity.[9]

The application of light-mediated ruthenium complexes can be divided into two categories: photodynamic therapy (PDT) and photoactivated chemotherapy (PACT).[10] PDT relies mainly on the generation of toxic reactive oxygen species (ROS), such as singlet oxygen ($^1O_2$). In contrast, PACT exploits different mechanisms to induce cell death, such as ligand ejection to create metal centers able to form DNA adducts, or photocaging approaches. In this article, we present the investigation of strained and unstrained ruthenium(II) complexes with 2-(2-pyridyl)benzazole ligands as promising antitumor agents, with possible application in both PDT and PACT.

[a] *Department of Chemistry, University of Kentucky, 505 Rose Street, Lexington, Kentucky 40506, USA*
E-mail: ec.glazer@uky.edu
http://glazerlab.as.uky.edu/

Supporting information and ORCID(s) from the author(s) for this article are available on the WWW under http://dx.doi.org/10.1002/ejic.201601450.

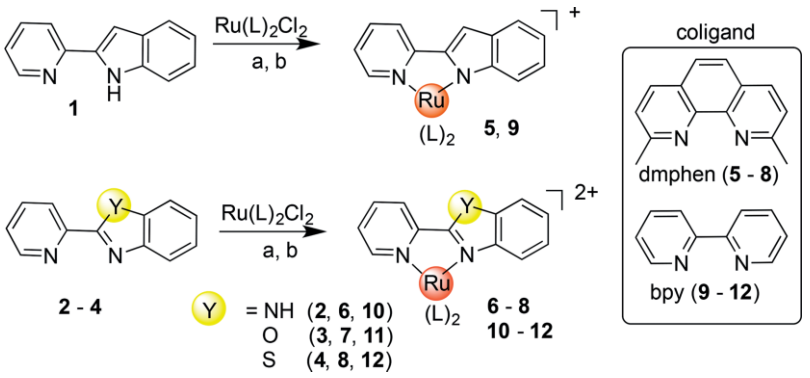

Scheme 1. Synthesis of Ru^{II} complexes with bioisosteric 2-(2-pyridyl)benzazole ligands. Reagents, conditions and yields: (a) $Ru(dmphen)_2Cl_2$ (1.0 equiv.), ethylene glycol, 100–120 °C for 2 h (**5**–**8**), 20–30 %; (b) $Ru(bpy)_2Cl_2$ (1.0 equiv.), ethanol/water (1:1), 90 °C for 2 h (**9**–**12**), 45–95 %.

The benzazole moiety was chosen, as it combines features, including extended conjugation for modulation of the absorption profile, and the potential for intrinsic steric clash within a coordination complex, similar to quinoline-containing ligands.[8b] It also facilitated a systematic investigation, as it provided a single point for chemical variation, with a heteroatom (N, O, S) at the 1-position, with a nitrogen atom at the 3-position, or a carbon atom at the analogous position in indole (Scheme 1). Moreover, benzazole-containing systems exhibit a variety of biological activities and applications. Recently, organometallic systems containing this ligand type have been explored, including half-sandwich (arene)ruthenium(II) compounds with pyridylbenzimidazole ligands studied for their DNA binding ability,[11] cyclin-dependent kinase (CDK1) inhibitory effects,[11b] and inhibition of protein tyrosine phosphatase (PTP-1B).[12] The previous investigations of ruthenium complexes with arylbenzimidazole ligands showed cytotoxic effects at μM concentrations.[11b,13]

In this report, we have discovered that coordination of non-cytotoxic 2-(2-pyridyl)benzazole ligands with an $Ru(dmphen)_2$ (dmphen = 2,9-dimethyl-1,10-phenanthroline) scaffold, forming strained Ru^{II} complexes, promoted significant cytotoxic potential of compounds with single-digit μM IC_{50} values, both under dark and light conditions. In contrast, the complexes with 2,2′-bipyridine (bpy) ligands were not active in the absence of light. However, these compounds were effective in killing cells when irradiated, producing nM IC_{50} values. DNA damage analysis and evaluation of singlet-oxygen production confirmed that unstrained compounds generate toxic ROS. However, the disparity in the effective concentration and trends for cytotoxicity (IC_{50} < 1 μM) and singlet-oxygen generation (> 10 μM) suggests that these compounds act through some additional, currently unknown, mechanism(s) of action.

Results and Discussion

Synthesis and Characterization

To explore structure–activity relationships (SAR), a small family of heteroleptic Ru^{II} complexes (**5**–**12**), containing one 2-(2-pyridyl)benzazole-type ligand and two strain-inducing dmphen ligands or two bpy ligands, were synthesized, as shown in Scheme 1. Four heterocyclic bioisosteres were studied: 2-(2-pyridyl)indole (pi) (**1**), 2-(2-pyridyl)benzimidazole (pbi) (**2**), 2-(2-pyridyl)benzoxazole (pbo) (**3**), and 2-(2-pyridyl)benzothiazole (pbt) (**4**). These systems were chosen to investigate the impact of replacing one pyridyl-type ligand with a benzazole on the cytotoxicity and photochemical properties of the Ru^{II} complexes.

The Ru^{II} complexes were synthesized from a racemic mixture of the Δ and Λ enantiomers of $Ru(dmphen)_2Cl_2$ or $Ru(bpy)_2Cl_2$, and thus, they form a mixture of enantiomers upon coordination of the pyridylbenzazole ligands. All complexes were exhaustively purified to ensure no contamination of either free ligands or coordinatively unsaturated Ru^{II} centers. As the pyridylindole is deprotonated, the complexes carry a +1 charge; all other complexes have a charge of +2. The complexes were characterized by ^1H NMR spectroscopy, ESI mass spectrometry, X-ray crystallography, and UV spectroscopy (see Figures S6–S10, S18–S27 in the Supporting Information). The strained complexes **5**–**8** were synthesized and characterized for the first time; the unstrained complexes **9**–**12** have been described previously.[14] In contrast to the described ^1H NMR spectra (300 MHz, CD_3CN) for **11** and **12**,[14b] we observed that some resonances for H4 and H5 of the bpy coligands were resolved as doublets of doublets of doublets (ddd).[15]

X-ray Crystallography

The structures of complexes **6**–**8** were determined by X-ray crystallography and are shown in Figure 1. Selected bond lengths and angles are listed in Table 1.

As expected, complexes **6**–**8** exhibited distorted octahedral geometries. Incorporation of two dmphen ligands resulted in the Ru–N bond lengthening to 2.108 Å (average value for **6**), 2.103 Å (average value for **7**), and 2.105 Å (average value for **8**), in comparison with 2.040–2.059 Å for the corresponding complexes with bpy coligands.[14b,16] The bond length to the pyridine ring (Ru–N5) is shorter in the pbo and pbt ligands, than

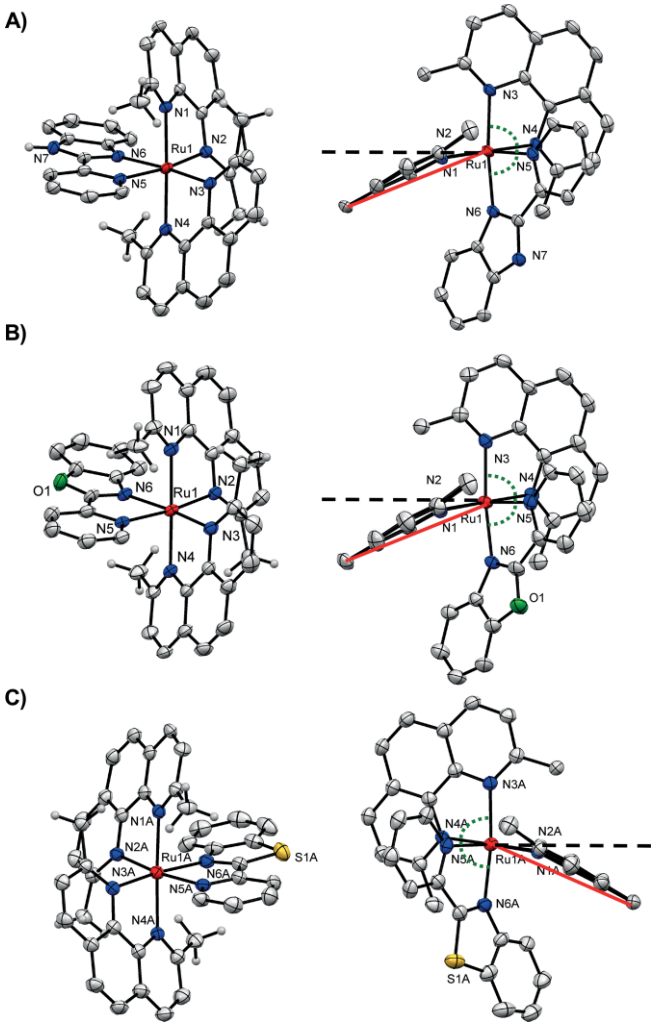

Figure 1. Ellipsoid plot of ruthenium complexes: (A) (*Δ*)-**6**, (B) (*Δ*)-**7**, (C) (*Λ*)-**8** at 50 % probability with H atoms omitted for clarity. Right column: side views, highlighting the distortion of the dmphen ligand. The black dashed lines indicate the normal plane and the angle between the red line and the black dashed line represents the ligand bend. Note: for **8** only, one cation of the asymmetric unit is shown.

the bond to the benzazole ring, while the Ru–N6 bond to the benzimidazole is shorter than that to the pyridine ring in **6** (Table 1). In contrast to complexes containing the 2,2′-biquinoline ligand,[8b] the two-ring systems in the benzazole-containing ligands are essentially coplanar, and do not contribute significantly to the distortion in the complexes.

The bond angles between dmphen ligands are non-equivalent, with the largest distortion from the ideal 90° and 180° for complex **8**. These deviations are larger than for unstrained compound **11** (Figure S5).[14b] Both the dmphen ligands (L1 and L2; Figure 1, Table 1) for each compound **6**–**8** are considerably bent from the normal plane, with deviations of 19.5–22.7°. Although the bend angle for L1 is the same for all complexes, the bends of L2 are not equivalent for **6**–**8**, creating variations in strain in the molecules that could cause the difference in photoejection kinetics (Table 2).

Table 1. Selected bond lengths [Å], bond angles [°] and torsion angles [°] of **6**–**8**.

	6	**7**	**8**
Bond lengths [Å]			
Ru-N1	2.114(3)	2.114(3)	2.114(2)
Ru-N2	2.097(3)	2.103(3)	2.102(2)
Ru-N3	2.100(3)	2.090(3)	2.097(2)
Ru-N4	2.120(3)	2.105(3)	2.108(2)
Ru-N5	2.109(3)	2.106(3)	2.097(2)
Ru-N6	2.099(3)	2.112(3)	2.112(2)
Bond angles [°]			
N1–Ru–N2	79.45(11)	79.73(10)	79.06(9)
N1–Ru–N3	100.6(1)	100.96(11)	101.40(9)
N1–Ru–N4	178.35(11)	178.86(11)	177.52(9)
N1–Ru–N5	95.9(1)	95.99(10)	96.07(9)
N1–Ru–N6	81.86(10)	80.24(11)	82.05(9)
N2–Ru–N3	94.57(10)	94.56(10)	93.35(9)
N2–Ru–N4	102.1(1)	100.78(10)	103.19(9)
N2–Ru–N5	170.3(1)	171.59(10)	171.30(9)
N2–Ru–N6	92.78(10)	94.05(10)	94.03(9)
N3–Ru–N4	79.88(11)	80.04(11)	79.62(9)
N3–Ru–N5	94.66(10)	93.36(10)	94.69(9)
N3–Ru–N6	172.56(10)	171.39(10)	172.34(9)
N4–Ru–N5	82.49(10)	83.38(10)	81.57(9)
N4–Ru–N6	97.46(10)	98.69(10)	96.67(9)
N5–Ru–N6	78.06(10)	78.02(10)	78.07(10)
Torsion angles [°]			
N1–C6–C7-N2	2.1(4)	1.2(5)	–2.2(4)
Ru–N1–C2–C3	–167.4(3)	–167.1(3)	163.2(2)
Ru–N2–C11–C10	164.0(2)	165.9(3)	–162.8(2)
N3–C20–C21–N4	1.8(5)	2.0(4)	–4.0(4)
Ru–N3–C16–C17	169.4(3)	168.7(3)	–171.0(2)
Ru–N4–C25–C24	–165.6(2)	–167.8(2)	162.3(2)
N5–C33–C34–N6	1.8(4)	3.0(5)	–2.3(4)
Ru–N5–C29–C30	176.0(3)	175.3(3)	–177.4(2)
L1 bend[a]	22.6	22.6	22.7
L2 bend[b]	21.4	19.5	21.6

[a] L1 bend = average angle (N3–Ru–C13/C14) – 90°; L1: dmphen where L is N1 and N2. [b] L2 bend = average angle (N2–Ru–C27/C28) – 90°; L2: dmphen where L is N3 and N4.

Table 2. Photophysical and photochemical properties for **5**–**12** under various reaction conditions.[a]

Compound	λ_{max} [nm]		$t_{1/2}$ [min]	
	Water	Opti-MEM	Water	Opti-MEM
5	475	475	47.3 ± 2.80	n.r.[a]
6	455	455	1.17 ± 0.08	10.38 ± 0.33
7	450	450	1.03 ± 0.09	1.42 ± 0.04
8	440	440	0.34 ± 0.04	0.66 ± 0.002
9	490	490	66.02 ± 13.11	66.11 ± 5.95
10	455	435	n.r.	n.r.
11	450	450	n.r.	n.r.
12	445	450	n.r.	n.r.

[a] n.r. = no reaction.

Photochemistry

The photochemical reaction of strained Ru^{II} complexes **5**–**9** were monitored by absorption spectroscopy, and exhibited selective photoejection of one ligand when irradiated with > 450 nm light, as shown in Figure 2A and Figures S6–S10. The

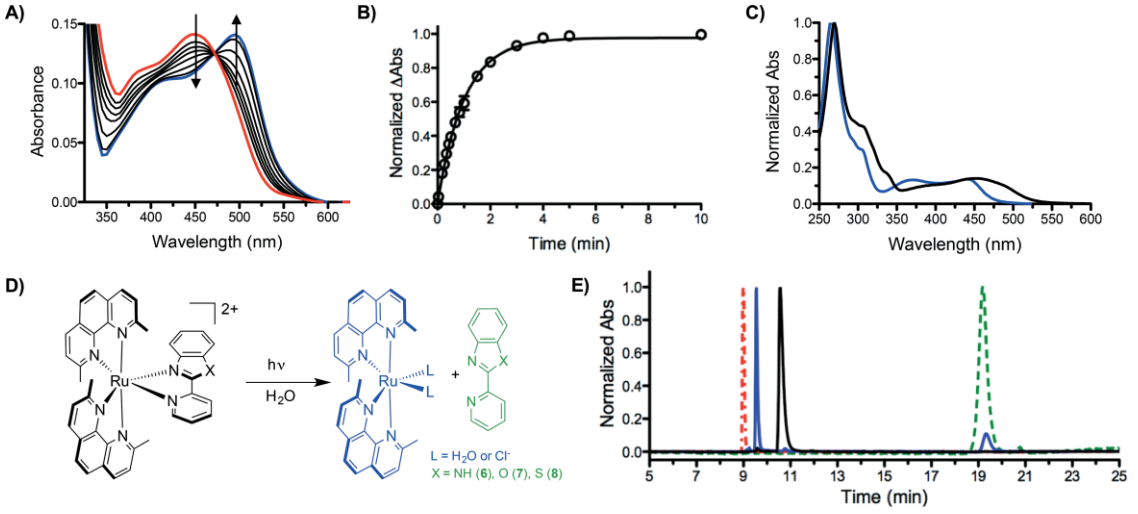

Figure 2. (A) Photoejection of **7** (30 μM) in water for 0–10 min irradiation, followed by UV/Vis absorption; red = initial, blue = final. (B) The photoejection kinetics for **7**; reaction was complete in less than 5 min. (C) Determination of photoejection products by HPLC: absorption profile of **7** (black, retention time = 10.56 min) and the photochemical product (blue, retention time = 9.55 min); note that the presence of CH_3CN changes the absorption profile; see Figure S28). (D) Photoejection reaction scheme for **6**–**8**, showing the photochemical products. (E) HPLC chromatogram of **7** before (black) and after irradiation for 1 min with the Indigo LED (blue), in comparison with started ligands: dmphen (red) and pbo (green). The same light dose was used in the cell studies.

presence of an isosbestic point indicated the direct conversion into a single product (Figure 2A). The half-life ($t_{1/2}$) of ligand ejection in water for **6**–**8** is 40–140 times faster than for **5**.

Complex **8** exhibited the fastest ejection, and also the largest bend of the dmphen ligand (L2; Table 1), indicating a correlation between the strain in the complex and the photochemical properties. The half-life was also found to be sensitive to the environment, as compound **6** demonstrated a ninefold slower ligand ejection in Opti-MEM, the media used in tissue culture experiments, than in water (Table 2).

The selective ejection of the 2-(2-pyridyl)benzazole ligands after irradiation of **6**–**8** in water was confirmed by HPLC by comparison with the starting complex and ligands (Figure 2E; the same light dose was used as in the cell experiments). Most unstrained Ru^{II} complexes with bpy coligands (**10**–**12**) did not eject after 4 h of irradiation, but complex **9** gave a $t_{1/2}$ value of 66 min (Table 2).

Cytotoxicity, SAR, and DNA Damage

An SAR study was performed for 2-(2-pyridyl)benzazole ligands, based on benzazole core bioisosterism and the corresponding Ru^{II} complexes with dmphen or bpy coligands. None of the free ligands exhibited activity against a leukemic cell line (HL60 human promyelocytic leukemia) for concentrations up to 100 μM (Figure 3, Table 3). Compounds **5**–**8** were 20–300-fold more potent against the HL60 cell line than the parent ligands, with IC_{50} values ranging from 0.34 to 4.55 μM. Unexpectedly, the photoreactive compounds **6**–**8** exhibited the same range of activity under dark and light conditions. However, the strained Ru^{II} complexes exhibited a steeper dose response when light-activated, and caused essentially complete cell death in lower concentrations (Figure 3A).

For the photoejecting systems, the largest phototoxicity index (PI) value was found for complex **5**, which produced a 10-fold enhanced activity upon irradiation, with a 34 nM IC_{50} value (Table 3). The highest PI values were found for **10**–**12**, which contain the $Ru(bpy)_2$ scaffold. After irradiation, compounds **9**, **10**, and **12** produced sub-μM IC_{50} values, with 7–220-fold differences in the light and dark, and demonstrated 3–17-fold greater potencies than cisplatin. The 88-fold (**12**; Figure S13) and 224-fold (**10**; Figure 3B) difference in light and dark IC_{50} values provides a large potential therapeutic window to allow for selective targeting of cells by exposure to light.

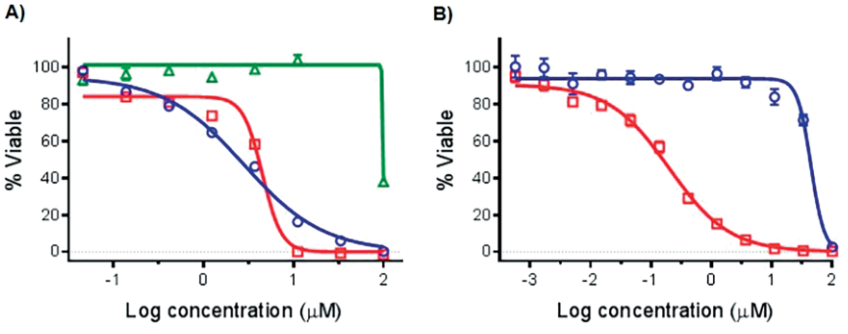

Figure 3. Cytotoxicity dose responses of ruthenium complexes and parent ligand on HL60 cells: (A) **2** and **6**, (B) **10**. Dark conditions (circles, blue line); irradiated samples, 1 min of > 450 nm light using the Indigo LED (29.1 J cm^{-2}; squares, red line); ligand **2** (triangles, green line) (n = 3).

Table 3. Cytotoxicity IC_{50} values for 2-(2-pyridyl)benzazole ligands and Ru complexes in the HL60 cancer cell line.

Compound	Coligand	Y	Dark IC_{50} [μM]	Light[a] IC_{50} [μM]	PI
1	–	CH	> 100	n.d.[b]	n.d.
2	–	NH	> 100	n.d.	n.d.
3	–	O	> 100	n.d.	n.d.
4	–	S	> 100	n.d.	n.d.
5	dmphen	CH	0.34 (±0.008)	0.034 (±0.001)	10
6	dmphen	NH	2.79 (±0.31)	4.49 (±0.07)	0.6[c]
7	dmphen	O	4.54 (±1.37)	3.43 (±0.75)	1.3
8	dmphen	S	1.55 (±0.41)	4.55 (±1.73)	0.3[c]
9	bpy	CH	1.24 (±0.008)	0.18 (±0.001)	7.3
10	bpy	NH	44.8 (±0.4)	0.20 (±0.017)	224
11	bpy	O	63.5 (±8.3)	5.18 (±0.047)	12.2
12	bpy	S	83.3 (±1.2)	0.94 (±0.09)	88
Cisplatin	–	–	3.1 (±0.2)	3.1 (±0.2)	1

[a] Using the Loctite Indigo LED array (light dose of 29.1 J cm^{-2}). [b] n.d.: not determined. [c] The PI values reflect differences in the slopes of the dose response curves, and likely indicate that different cytotoxicity mechanisms are responsible for cell death under dark vs. light conditions.

The SAR study revealed the following: (1) coordination of 2-(2-pyridyl)benzazole ligands with the Ru^{II} scaffolds is crucial for potency; (2) the cytotoxic effect is sensitive to the coligands (dmphen vs. bpy) – replacement of dmphen with bpy decreased the potency in the dark, but promoted nM activity after light irradiation (compounds **9**, **10**, **12**) and provided a large potential therapeutic window (88 for **12** and > 220 for **10**); (3) the nature of the benzazole core had an influence on the antitumor activity, with complexes **5** and **9** exhibiting 5–35-fold greater potency under dark conditions than other compounds from the strained and unstrained groups, respectively (Table 3, Figure 4). Notably, complexes **5** and **9** carry a +1 charge, while all other compounds carry +2.

The effect of the compounds **8** and **12** on the cell cycle was analyzed at the IC_{50} of the compounds over several time points (Figures S15 and S16). At the 24 h time point, the sub-G1 phase had increased to 45 % of the population for **8** and 27 % for **12** when the compounds had been irradiated. No significant increase in the population of apoptotic cells and the G1, S, or G2/M populations occurred for **8** and **12** in the dark. Thus, neither compound induced cell-cycle arrest under dark conditions or upon irradiation.

In an attempt to determine a potential mechanism of action, DNA damage was assessed by agarose gel electrophoresis. Supercoiled pUC19 plasmid was incubated with each complex in a dose-response study and kept in the dark or exposed to 470 nm light for 1 h (Figure 5). The irradiated samples revealed significant differences in damage profiles. The strained photoactive Ru^{II} complexes **6** and **8** exhibited a combination of DNA photocleavage and DNA photobinding (Figure 5A and B). Covalent adducts were visualized by the reduced mobility on the agarose gel with increasing concentration of Ru^{II} complex, as well as a loss of the EtBr signal. Unstrained complex **12** induced single-strand breaks in the DNA when irradiated with light, likely due to the photogeneration of $^1O_2$. This was visualized by the conversion from supercoiled DNA to relaxed circle (Figure 5D). Unexpectedly, unstrained **10** produced fewer single-strand breaks than **12**, based on the small ratio between relaxed circle and supercoiled DNA (Figure 5C). Precipitation of the DNA with the complexes **5**, **8**, and **9** was observed at concentrations above 125 μM.

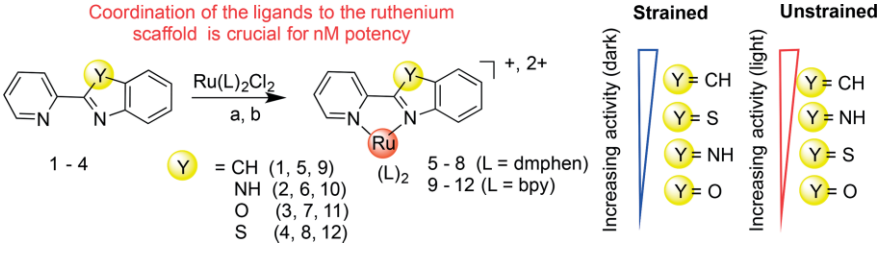

Figure 4. SAR analysis for antitumor Ru^{II} complexes with 2-(2-pyridyl)benzazole ligands.

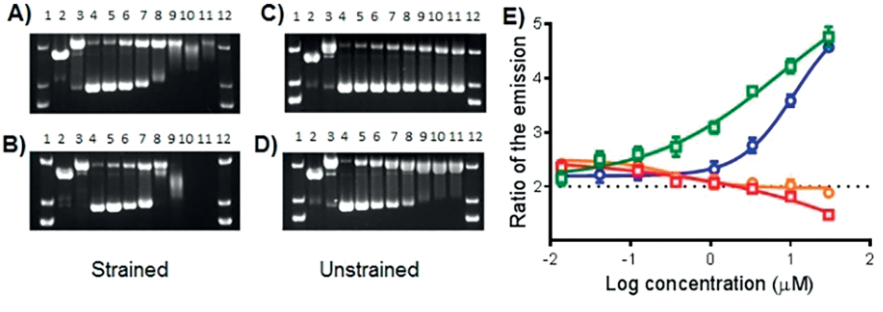

Figure 5. Agarose gel electrophoresis of pUC19 plasmid (40 μg mL^{-1}; 10 mM phosphate buffer, pH 7.5) with light-activated Ru^{II} compounds. Dose response profiles: (A) **6**, (B) **8**, (C) **10**, (D) **12**; lanes 1 and 12, DNA molecular weight standard; lane 2, linear pUC19; lane 3, relaxed circle [$Cu(phen)_2$ reaction with pUC19]; lanes 4–11, 0, 7.8, 15.6, 31.25, 62.5, 125, 250, and 500 μM compound. (E) Singlet-oxygen generation dose responses of ruthenium complexes: **6** (circles, orange line), **8** (squares, red line), **10** (circles, blue line), and **12** (squares, green line) (n = 2). The data are shown as a ratio of the emission of the sensor after irradiation with the compound vs. without irradiation. The slight downward curve for **8** suggests this compound quenches singlet oxygen at high doses.

Despite the difference in their ability to inflict DNA damage, both the unstrained compounds **10** and **12** induced sub-μM cytotoxicity after light irradiation and exhibited large PI values. In an attempt to confirm or disprove the involvement of light-activated generated $^1O_2$ in the biological mechanism of action, dose responses of compounds were performed with singlet-oxygen sensor green reagent with light irradiation (Figure 5E; Figure S15). As anticipated, photogeneration of $^1O_2$ was observed for both unstrained complexes **10** and **12**, in contrast to the corresponding strained compounds **6** and **8**. Consistent with the DNA damage gels, compound **12** exhibited greater potency for $^1O_2$ generation; however, there is a large discrepancy between the concentrations needed to produce $^1O_2$ or induce strand breaks in the DNA, compared with cytotoxicity IC_{50} values. This suggests that $^1O_2$ alone cannot be responsible for the potent effects in cells.[17] Moreover, the pyridylindole-based complexes (**5** and **9**) possessed the highest cytotoxicity and did not generate $^1O_2$ upon irradiation (Figure S15).

Conclusion

Eight heteroleptic Ru^{II} complexes were synthesized in order to explore structure–activity relationships. The complexes contained one 2-(2-pyridyl)benzazole-type ligand, combined with either two dmphen ligands to make intrinsically strained complexes, or two 2,2′-bipyridine ligands to form unstrained complexes. While the free benzazole-type ligands **1**–**4** were not toxic in the investigated concentration range, the Ru^{II} complexes exhibited marked cytotoxicity. The most potent compounds, **5** and **9**, contained the 2-(2-pyridyl)indole ligand and were highly effective in killing leukemic cells when irradiated, with IC_{50} values less than 0.04 and 0.2 μM. However, the observed high toxicity in the dark could be a limitation for their potential application as PDT agents.

In contrast, large therapeutic windows were found for complexes **12** and **10** (with 88- and 224-fold differences in their light and dark IC_{50} values), which demonstrated 3–15-fold greater potency than cisplatin. The unstrained compounds are capable of generating singlet oxygen, but the significant disparity in the effective concentration for cytotoxicity, $^1O_2$ production, and DNA cleavage suggests that some other, currently unknown, mechanisms of action could be involved for anticancer activity. This may involve different species of ROS.

Considering the promising dark cytotoxicity of strained complexes and light-induced antitumor potential of unstrained compounds, we are currently modifying these complexes, aiming to generate more potent anticancer agents with possible applications in both standard chemotherapy and photodynamic therapy.

Experimental Section

Materials and Methods: The starting 2-(2-pyridyl)benzazole ligands were obtained from commercial sources (**2**, **3**) or were synthesized according to the methods described previously (**1**, **4**).[18] Complexes **10**–**12** were synthesized using previously established procedures.[14] All ^1H NMR spectra were obtained with a Varian Mercury spectrometer (400 MHz) with chemical shifts reported relative to the residual solvent peak of acetonitrile at δ = 1.94 ppm. Electrospray ionization mass spectra were obtained with a Varian 1200L mass spectrometer. Absorption spectra were obtained with an Agilent Cary 60 spectrophotometer or a BMG Labtech FLUOstar Omega microplate reader. Photoejection, DNA damage, and singlet-oxygen generation experiments were performed using a 470 nm LED array from Elixa and a Loctite Indigo LED array (for cell cytotoxicity studies and HPLC photoejection analysis). All synthesized compounds were isolated in > 95 % purity, as determined by analytical HPLC. For HPLC analysis, the ruthenium complexes were injected into an Agilent 1100 series HPLC equipped with a model G1311 quaternary pump, G1315B UV diode array detector, and ChemStation software version B.01.03. Chromatographic conditions were optimized with a Column Technologies Inc. C18, 120 Å (250 mm × 4.6 mm inner diameter, 5 μM), fitted with a Phenomenex C18 (4 mm × 3 mm) guard column. Injection volumes of 15 μL of 100 μM solutions of the complex were used. The detection wavelength was 280 nm. Mobile phases were: mobile phase A, formic acid (0.1 %) in distilled water (dH_2O); mobile phase B, formic acid (0.1 %) in HPLC grade acetonitrile. The mobile phase flow rate was 1.0 mL min^{-1}. The following mobile phase gradient was used: 98–95 % A (containing 2–5 % B) from 0 to 5 min; 95–70 % A (5–30 % B) from 5 to 15 min; 70–40 % A (30–60 % B) from 15 to 20 min; 40–5 % A (60–95 % B) from 20 to 30 min; 5–98 % A (95–2 % B) from 30 to 35 min; re-equilibration at 98 % A (2 % B) from 35 to 40 min.

General Procedure for the Synthesis of $Ru(dmphen)_2L$ Complexes with 2-(2-Pyridyl)benzazole Ligands: $Ru(dmphen)_2Cl_2$ (1 equiv.) and 2-(2-pyridyl)benzazole (1.1 equiv.) were added to ethylene glycol (4 mL) in a 15 mL pressure tube. The mixture was heated at 100–120 °C while protected from light for 2 h. The dark brown (**5**) or orange solution (**6**–**8**) was cooled to room temperature and poured into dH_2O (50 mL). Addition of a saturated aq. KPF_6 solution (ca. 1 mL) produced a brown or red-orange precipitate that was collected by vacuum filtration. The purification of the solid was carried out by flash chromatography [silica gel, loaded in KNO_3 (0.1 %), H_2O (5 %) in MeCN]. A gradient was run, and the pure complex was eluted at KNO_3 (0.2 %), H_2O (5–10 %) in MeCN. The product fractions were concentrated under reduced pressure, and a saturated aq. solution of KPF_6 was added, followed by extraction of the complex with CH_2Cl_2. The solvent was removed under reduced pressure to give a solid.

5: R_f = 0.63 [KNO_3 (0.1 %), H_2O (5 %) in MeCN]. ^1H NMR (CD_3CN): δ = 8.59 (d, J = 8.2 Hz, 1 H), 8.52 (d, J = 8.3 Hz, 1 H), 8.21 (d, J = 8.3 Hz, 1 H), 816 (d, J = 8.7 Hz, 1 H), 8.02–8.06 (m, 3 H), 7.81 (d, J = 8.7 Hz, 1 H), 7.74 (d, J = 8.3 Hz, 1 H), 7.70 (d, J = 8.0 Hz, 1 H), 7.64 (d, J = 8.3 Hz, 1 H), 7.44 (t, J = 7.8 Hz, 1 H), 7.32 (d, J = 8.3 Hz, 1 H), 7.28 (d, J = 8.3 Hz, 1 H), 7.20 (d, J = 8.0 Hz, 1 H), 6.93 (s, 1 H), 6.57 (d, J = 5.6 Hz, 1 H), 6.43–6.47 (m, 2 H), 6.13 (d, J = 7.5 Hz, 1 H), 4.47 (d, J = 8.5 Hz, 1 H), 2.02 (s, 3 H), 1.98 (s, 3 H), 1.85 (s, 3 H), 1.82 (s, 3 H) ppm. Purity by HPLC = 97 %. ESI-MS: calcd. for $C_{41}H_{33}N_6Ru$ $[M]^+$ 711.18; found 711.3. UV/Vis (CH_3CN): λ_{max} (ε, mol^{-1} dm cm–1) = 490 (8400) nm.

6: R_f = 0.38 [KNO_3 (0.1 %), H_2O (5 %) in MeCN]. ^1H NMR (CD_3CN): δ = 8.69 (d, J = 8.3 Hz, 1 H), 8.62 (d, J = 8.3 Hz, 1 H), 8.30 (d, J = 8.3 Hz, 1 H), 8.23 (d, J = 8.8 Hz, 1 H), 8.09–8.15 (m, 3 H), 8.00 (d, J = 7.9 Hz, 1 H), 7.82–7.88 (m, 3 H), 7.72 (d, J = 8.3 Hz, 1 H), 7.36–7.43 (m, 3 H), 7.15 (t, J = 7.4 Hz, 1 H), 6.93–7.00 (m, 3 H), 6.72 (ddd, J = 8.8, 7.3, 0.9 Hz, 1 H), 4.91 (d, J = 8.5 Hz, 1 H), 1.98 (s, 3 H), 1.95 (s, 3 H), 1.91 (s, 3 H), 1.88 (s, 3 H) ppm. Purity by HPLC = 97 %. ESI-MS:

calcd. for $C_{40}H_{33}N_7Ru$ $[M]^{2+}$ 356.59; found 356.7. UV/Vis (CH_3CN): λ_{max} (ε, mol^{-1} dm cm–1) = 455 (11800) nm.

7: R_f = 0.52 [KNO_3 (0.1 %), H_2O (5 %) in MeCN]. ^1H NMR (CD_3CN): δ = 8.74 (d, J = 8.3 Hz, 1 H), 8.68 (d, J = 8.3 Hz, 1 H), 8.35 (d, J = 8.3 Hz, 1 H), 8.27 (d, J = 8.7 Hz, 1 H), 8.23 (d, J = 8.3 Hz, 1 H), 8.13–8.20 (m, 3 H), 7.94–7.98 (m, 2 H), 7.86 (d, J = 8.3 Hz, 1 H), 7.78 (d, J = 8.4 Hz, 1 H), 7.66 (d, J = 8.5 Hz, 1 H), 7.40–7.46 (m, 3 H), 7.16 (ddd, J = 8.0, 5.8, 1.5 Hz, 1 H), 7.00–7.04 (m, 2 H), 5.12 (d, J = 8.3 Hz, 1 H), 2.11 (s, 3 H), 2.00 (s, 3 H), 1.98 (s, 3 H), 1.90 (s, 3 H) ppm. Purity by HPLC = 98 %. ESI-MS: calcd. for $C_{40}H_{32}N_6ORu$ $[M^{2+}{\cdot}PF_6^-]^+$ 859.13; found 859.3. ESI-MS: calcd. for $C_{40}H_{32}N_6ORu$ $[M]^{2+}$ 357.09; found 356.9. UV/Vis (CH_3CN): λ_{max} (ε, mol^{-1} dm cm–1) = 445 (7700) nm.

8: R_f = 0.51 [KNO_3 (0.1 %), H_2O (5 %) in MeCN]. ^1H NMR (CD_3CN): δ = 8.72 (d, J = 8.3 Hz, 1 H), 8.67 (d, J = 8.3 Hz, 1 H), 8.41 (d, J = 8.3 Hz, 1 H), 8.28 (d, J = 8.8 Hz, 1 H), 8.23 (d, J = 8.4 Hz, 1 H), 8.16–8.20 (m, 2 H), 8.08 (d, J = 8.8 Hz, 1 H), 7.91–7.95 (m, 2 H), 7.89 (d, J = 8.4 Hz, 1 H), 7.84 (d, J = 8.7 Hz, 1 H), 7.73 (d, J = 8.4 Hz, 1 H), 7.49 (d, J = 8.3 Hz, 1 H), 7.40 (d, J = 8.4 Hz, 1 H), 7.34 (ddd, J = 8.8, 7.4, 1.0 Hz, 1 H), 7.09–7.14 (m, 2 H), 6.92 (ddd, J = 8.8, 7.1, 1.2 Hz, 1 H), 5.37 (d, J = 8.6 Hz, 1 H), 2.10 (s, 3 H), 2.01 (s, 3 H), 1.85 (s, 3 H), 1.84 (s, 3 H) ppm. Purity by HPLC = 99 %. ESI-MS: calcd. for $C_{40}H_{32}N_6RuS$ $[M^{2+}{\cdot}PF_6^-]^+$ 875.11; found 875.3. ESI-MS: calcd. for $C_{40}H_{32}N_6RuS$ $[M]^{2+}$ 365.08; found 365.1. UV/Vis (CH_3CN): λ_{max} (ε, mol^{-1} dm cm–1) = 445 (8900) nm.

General Preparation of the Ru(bpy)$_2$L Complexes: $Ru(bpy)_2Cl_2{\cdot}2H_2O$ (120 mg, 0.23 mmol) and 2-(2-pyridyl)benzazole (0.27 mmol) were added to EtOH/H_2O (50:50; 6 mL) in a 15 mL pressure tube. The mixture was heated at 90 °C for 2 h, after which the orange solution was cooled to room temperature. Addition of a saturated aq. KPF_6 solution resulted in the precipitation of the complex, which was extracted with dichloromethane. Purification of the orange solid was carried out by flash chromatography [silica gel, loaded in KNO_3 (0.1 %), H_2O (5 %) in MeCN]. The pure complex eluted at 0.2 % KNO_3, 10 % H_2O in MeCN, and the product fractions were concentrated under reduced pressure. A saturated aq. solution of KPF_6 was added, and the complex was extracted with CH_2Cl_2, followed by removal of the solvent under reduced pressure to give an orange solid.

9: R_f = 0.60 [KNO_3 (0.1 %), H_2O (5 %) in MeCN]. ^1H NMR (CD_3CN): δ = 8.40–8.44 (m, 3 H), 8.30 (d, J = 8.2 Hz, 1 H), 7.92–8.01 (m, 5 H), 7.88 (td, J = 8.0, 1.5 Hz, 1 H), 7.75–7.90 (m, 2 H), 7.69 (ddd, J = 8.2, 7.5, 1.6 Hz, 1 H), 7.55 (ddd, J = 6.0, 1.6, 0.8 Hz, 1 H), 7.46 (dt, J = 8.0, 1.0 Hz, 1 H), 7.31–7.35 (m, 3 H), 7.19–7.27 (m, 3 H), 6.89 (ddd, J = 8.0, 5.8, 1.6 Hz, 1 H), 6.68 (ddd, J = 8.0, 6.8, 0.8 Hz, 1 H), 6.47 (ddd, J = 8.8, 6.8, 1.2 Hz, 1 H), 5.38 (d, J = 7.5 Hz, 1 H) ppm. Purity by HPLC = 98 %. ESI-MS: calcd. for $C_{33}H_{25}N_6Ru$ $[M]^+$ 607.12; found 607.1. UV/Vis (CH_3CN): λ_{max} (ε, mol^{-1} dm cm–1) = 480 (8600) nm.

10: R_f = 0.38 [KNO_3 (0.1 %), H_2O (5 %) in MeCN]. ^1H NMR (CD_3CN): δ = 8.51–8.54 (m, 3 H), 8.47 (d, J = 8.1 Hz, 1 H), 8.44 (d, J = 8.1 Hz, 1 H), 7.96–8.15 (m, 6 H), 7.80–7.87 (m, 3 H), 7.71–7.75 (m, 2 H), 7.47 (ddd, J = 8.0, 5.6, 1.3 Hz, 1 H), 7.37–7.44 (m, 4 H), 7.34 (ddd, J = 8.0, 5.6, 1.2 Hz, 1 H), 7.05 (ddd, J = 8.8, 7.4, 1.1 Hz, 1 H), 5.82 (d, J = 8.3 Hz, 1 H) ppm. Purity by HPLC = 99 %. ESI-MS: calcd. for $C_{32}H_{25}N_7Ru$ $[M]^{2+}$ 304.56; found 304.6. UV/Vis (CH_3CN): λ_{max} (ε, mol^{-1} dm cm–1) = 455 (13100) nm.

11: R_f = 0.45 [KNO_3 (0.1 %), H_2O (5 %) in MeCN]. ^1H NMR (CD_3CN): δ = 8.51–8.54 (m, 3 H), 8.48 (d, J = 7.9 Hz, 1 H), 8.45 (d, J = 8.2 Hz, 1 H), 8.01–8.19 (m, 6 H), 7.94 (d, J = 5.4 Hz, 1 H), 7.88 (d, J = 8.5 Hz, 1 H), 7.77–7.82 (m, 3 H), 7.61 (ddd, J = 8.8, 7.5, 1.1 Hz, 1 H), 7.55 (ddd, J = 8.0, 5.6, 1.3 Hz, 1 H), 7.42–7.49 (m, 3 H), 7.39 (ddd, J = 8.0, 5.6, 1.2 Hz, 1 H), 7.28 (ddd, J = 8.8, 7.6, 0.9 Hz, 1 H), 5.96 (d, J = 8.2 Hz, 1 H) ppm. Purity by HPLC = 95 %. ESI-MS: calcd. for $C_{32}H_{25}N_6ORu$ $[M]^{2+}$ 305.06; found 305.1. UV/Vis (CH_3CN): λ_{max} (ε, mol^{-1} dm cm–1) = 450 (12600) nm.

12: R_f = 0.45 [KNO_3 (0.1 %), H_2O (5 %) in MeCN]. ^1H NMR (CD_3CN): δ = 8.51–8.54 (m, 4 H), 8.44 (d, J = 8.1 Hz, 1 H), 8.20 (d, J = 8.1 Hz, 1 H), 8.04–8.16 (m, 4 H), 8.01 (td, J = 8.0, 1.4 Hz, 1 H), 7.92 (d, J = 5.8 Hz, 1 H), 7.84 (d, J = 5.2 Hz, 1 H), 7.74 (d, J = 5.7 Hz, 1 H), 7.69 (d, J = 5.5 Hz, 1 H), 7.67 (d, J = 5.3 Hz, 1 H), 7.57 (ddd, J = 8.4, 7.2, 1.0 Hz, 1 H), 7.45–7.49 (m, 2 H), 7.37–7.42 (m, 2 H), 7.35 (ddd, J = 8.0, 5.6, 1.2 Hz, 1 H), 7.27 (ddd, J = 8.8, 7.3, 1.1 Hz, 1 H), 6.31 (d, J = 8.5 Hz, 1 H) ppm. Purity by HPLC = 98 %. ESI-MS: calcd. for $C_{32}H_{24}N_6RuS$ $[M^{2+}{\cdot}PF_6^-]^+$ 771.05; found 771.2. ESI-MS: calcd. for $C_{32}H_{24}N_6RuS$ $[M]^{2+}$ 313.04; found 313.1. UV/Vis (CH_3CN): λ_{max} (ε, mol^{-1} dm cm–1) = 445 (13100) nm.

Counterion Exchange: Compounds **5**–**12** were converted into Cl^- salts by dissolving the product (5–20 mg) in methanol (1–2 mL). The dissolved product was loaded onto an Amberlite IRA-410 chloride ion exchange column, eluted with methanol, and the solvent was removed in vacuo.

Cytotoxicity Assay: HL60 cells were plated at 30000 cell per well in extracellular solution (10 mM HEPES pH 7.5, 145 mM NaCl, 10 mM glucose, 1.2 mM $CaCl_2$, 1.2 mM $MgCl_2$, 3.3 mM KH_2PO_4, 0.8 mM K_2HPO_4, 50 U/mL penicillin and 50 µg/mL streptomycin) in 96-well plates. Compounds were serially diluted in a 96-well plate and then added to the cells. They were then irradiated with 29.1 J/cm^2 light (> 450 nm using the Indigo LED) for 1 min or kept in the dark. Following irradiation, an equal volume of opti-MEM with 2 % FBS was added. The cells were incubated with the compounds for 72 h followed by the addition of resazurin. The plates were incubated for 3 h and then read with a SpectraFluor Plus plate reader with an excitation filter of 535 nm and emission of 595 nm.

DNA Gel Electrophoresis: Compounds were mixed with pUC19 (40 µg mL^{-1}) plasmid DNA in potassium phosphate buffer (10 mM, pH 7.4). To determine the effect of light, samples were irradiated with a 470 nm LED for a total light dose of 46.8 J cm^{-2}. Samples were then incubated at room temperature in the dark for 12 h. Single- and double-strand DNA break controls were prepared, and the DNA samples were resolved on agarose gels, as described previously.[8a] In brief, samples were resolved on agarose gels (1 %) prepared in tris-acetate buffer with 0.3 µg of plasmid/lane. The gels were stained with ethidium bromide (0.5 µg mL^{-1}) in tris-acetate buffer at room temperature for 40 min, destained with tris-acetate buffer, and imaged with a ChemiDoc MP System (Bio-Rad).

Singlet-Oxygen Assay: Compounds were serially diluted in potassium phosphate buffer (10 mM, pH 7.4), with singlet-oxygen sensor green reagent (ca. 5 µM) in 96-well plates. The plates were read with a SpectraFluor Plus plate reader with an excitation filter of 485 nm and emission of 535 nm in the dark, and after 1 h irradiation with a 470 nm LED, for a total light dose of 46.8 J cm^{-2}.

Cell-Cycle Analysis: HL60 cells were plated in opti-MEM with FBS (1 %) at a density of 500000 cells mL^{-1} in 6-well plates. The compounds were added and incubated with the cells from 0 to 12 h. For each time point, the cells were transferred to FACS tubes, pelleted, washed with PBS, followed by the addition of cold ethanol (70 %) and incubated on ice for 1 h to fix the cells. Cells were then centrifuged at 2000 rpm for 5 min, and resuspended in PBS (1 mL) for each tube. The tubes were centrifuged at 2000 rpm for 5 min, the supernatant was aspirated and the cells were resuspended in PI (0.5 mL) staining buffer [PI (20 mg mL^{-1}) in PBS, RNAse (0.2 mg mL^{-1}), TritonX-100 (0.1 %)] and incubated at room tempera-

ture for 30 min. Samples were run through the flow cytometer, and data were analyzed with ModFit and FlowJo.

Crystallography: Single crystals of compounds **6**–**8** were grown from dichloromethane or acetone by vapor diffusion of diethyl ether. They were mounted in inert oil and transferred to the cold gas stream of the diffractometer. X-ray diffraction data were collected at 90.0(2) K with either a Nonius KappaCCD diffractometer using Mo-K_α X-rays or with a Bruker-Nonius X8 Proteum diffractometer with graded-multilayer-focused Cu-K_α X-rays. Raw data were integrated, scaled, merged, and corrected for Lorentz-polarization effects using either the HKL-SMN package[19] or the APEX2 package.[20] Corrections for absorption were applied using SADABS[21] and XABS2.[22] The structures were solved by SHELXT,[23] and refined against F^2 by weighted full-matrix least squares using SHELXL-2014.[24] For compound **8**, the SQUEEZE routine[25] was used to treat disordered solvent. Hydrogen atoms were placed at calculated positions and refined using a riding model. Non-hydrogen atoms were refined with anisotropic displacement parameters. Structures were checked using check CIF tools in Platon[26] and by an R-tensor.[27] Crystal data and selected details of the structure determinations are summarized below and selected geometrical parameters are given in Table 1.

Crystal Data (6): $C_{41}H_{35}Cl_2F_{12}N_7P_2Ru$, Mr = 1087.67, monoclinic, $P2_1/c$, a = 12.3286(2) Å, b = 18.7316(3) Å, c = 18.1692(3) Å, β = 94.943(1)°, V = 4180.29(12) Å^3, Z = 4, ϱ = 1.728 mg m^{-3}, μ = 5.802 mm^{-1}, $F(000)$ = 2184, crystal size 0.300 × 0.120 × 0.060 mm, θ(max) = 68.373°, 56392 reflections collected, 7596 unique reflections (R_{int} = 0.0433), GOF = 1.065, R_1 = 0.0408 and wR_2 = 0.0933 [$I > 2\sigma(I)$], R_1 = 0.0436 and wR_2 = 0.0949 (all indices), largest difference peak/hole = 1.531/–1.465 e Å^{-3}.

Crystal Data (7): $C_{48.29}H_{50.15}F_{12}N_6O_{3.50}P_2Ru$, Mr = 1161.55, monoclinic, $C2/c$, a = 23.0734(5) Å, b = 19.9646(5) Å, c = 22.6098(5) Å, β = 108.547(1)°, V = 9874.3(4) Å^3, Z = 8, ϱ = 1.563 mg m^{-3}, μ = 4.028 mm^{-1}, $F(000)$ = 4735, crystal size 0.230 × 0.180 × 0.030 mm, θ(max) = 68.355°, 60921 reflections collected, 8945 unique reflections (R_{int} = 0.0643), GOF = 1.036, R_1 = 0.0409 and wR_2 = 0.0985 [$I > 2\sigma(I)$], R_1 = 0.0561 and wR_2 = 0.1067 (all indices), largest difference peak/hole = 0.631/–0.544 e Å^{-3}.

Crystal Data (8): $C_{89}H_{82}F_{24}N_{12}O_3P_4Ru_2S_2$, Mr = 2213.80, triclinic, $P\bar{1}$, a = 14.2840(2) Å, b = 17.5165(2) Å, c = 20.0585(3) Å, α = 91.5547(8)°, β = 90.7709(8)°, γ = 110.9785(7)°, V = 4682.91(11) Å^3, Z = 2, ϱ = 1.570 mg m^{-3}, μ = 0.539 mm^{-1}, $F(000)$ = 2240, crystal size 0.320 × 0.280 × 0.270 mm, θ(max) = 27.509°, 136315 reflections collected, 21482 unique reflections (R_{int} = 0.0402), GOF = 1.054, R_1 = 0.0445 and wR_2 = 0.1153 [$I > 2\sigma(I)$], R_1 = 0.0688 and wR_2 = 0.1297 (all indices), largest difference peak/hole = 1.247/–0.749 e Å^{-3}.

CCDC 1532115 (for **6**), 1532116 (for **7**), 1532117 (for **8**) contain the supplementary crystallographic data for this paper. These data can be obtained free of charge from The Cambridge Crystallographic Data Centre.

Acknowledgments

This work was supported by the National Institutes of Health (5R01GM107586). The X8 Proteum was funded by the National Science Foundation (NSF) (MRI CHE-0319176). Mass spectrometry analysis was performed at the University of Kentucky Environmental Research Training Laboratory (ERTL).

Keywords: Synthesis · Photochemistry · Cytotoxicity · DNA damage · Ruthenium

[1] R. L. Siegel, K. D. Miller, A. Jemal, *Ca–Cancer J. Clin.* **2016**, *66*, 7–30.
[2] M. Galanski, M. A. Jakupec, B. K. Keppler, *Curr. Med. Chem.* **2005**, *12*, 2075–2094.
[3] a) M. J. Hannon, *Pure Appl. Chem.* **2007**, *79*, 2243–2261; b) A. M. Griffin, P. N. Butow, A. S. Coates, A. M. Childs, P. M. Ellis, S. M. Dunn, M. H. Tattersall, *Ann. Oncol.* **1996**, *7*, 189–195.
[4] a) E. S. Antonarakis, A. Emadi, *Cancer Chemother. Pharmacol.* **2010**, *66*, 1–9; b) N. P. Barry, P. J. Sadler, *Chem. Commun.* **2013**, *49*, 5106–5131.
[5] A. Bergamo, C. Gaiddon, J. H. Schellens, J. H. Beijnen, G. Sava, *J. Inorg. Biochem.* **2012**, *106*, 90–99.
[6] W. H. Ang, A. Casini, G. Sava, P. J. Dyson, *J. Organomet. Chem.* **2011**, *696*, 989–998.
[7] E. C. Glazer, *Isr. J. Chem.* **2013**, *53*, 391–400.
[8] a) B. S. Howerton, D. K. Heidary, E. C. Glazer, *J. Am. Chem. Soc.* **2012**, *134*, 8324–8327; b) E. Wachter, D. K. Heidary, B. S. Howerton, S. Parkin, E. C. Glazer, *Chem. Commun.* **2012**, *48*, 9649–9651; c) A. N. Hidayatullah, E. Wachter, D. K. Heidary, S. Parkin, E. C. Glazer, *Inorg. Chem.* **2014**, *53*, 10030–10032.
[9] D. K. Heidary, E. C. Glazer, *ChemBioChem* **2014**, *15*, 507–511.
[10] a) N. J. Farrer, L. Salassa, P. J. Sadler, *Dalton Trans.* **2009**, 10690–10701; b) C. Mari, V. Pierroz, S. Ferrari, G. Gasser, *Chem. Sci.* **2015**, *6*, 2660–2668.
[11] a) M.-A. M. Busto, J. M. Leal, A. M. Rodríguez, F. Domínguez, M. I. Acuña, G. Espino, B. García, *Organometallics* **2015**, *34*, 319–327; b) M. Martinez-Alonso, N. Busto, F. A. Jalon, B. R. Manzano, J. M. Leal, A. M. Rodriguez, B. Garcia, G. Espino, *Inorg. Chem.* **2014**, *53*, 11274–11288.
[12] J. X. Ong, C. W. Yap, W. H. Ang, *Inorg. Chem.* **2012**, *51*, 12483–12492.
[13] G. S. Yellol, A. Donaire, J. G. Yellol, V. Vasylyeva, C. Janiak, J. Ruiz, *Chem. Commun.* **2013**, *49*, 11533–11535.
[14] a) F. Wu, C. M. Chamchoumis, R. P. Thummel, *Inorg. Chem.* **2000**, *39*, 584–590; b) C. Richardson, F. R. Keene, P. J. Steel, *Aust. J. Chem.* **2008**, *61*, 183–188; c) H. Yi, J. A. Crayston, J. T. S. Irvine, *Dalton Trans.* **2003**, 685–691.
[15] W. Z. Shen, G. Trotscher-Kaus, B. Lippert, *Dalton Trans.* **2009**, 8203–8214.
[16] Y. J. Liu, H. Chao, H. J. Yu, Y. X. Yuan, L. N. Ji, *Acta Crystallogr., Sect. E: Struct. Rep. Online* **2006**, *62*, m585.
[17] Unfortunately, attempts to quantify the singlet oxygen using 1,3-diphenylisobenzofuran (DPBF) failed, due to poor stability of the reagent under irradiation. The procedure used was reported by: W. Zhang, B. Li, H. Ma, L. Zhang, Y. Guan, Y. Zhang, X. Zhang, P. Jing, S. Yue, *ACS Appl. Mater. Interfaces* **2016**, *8*, 21465–21471.
[18] a) G. Cravotto, F. Demartin, G. Palmisano, A. Penoni, T. Radice, S. Tollari, *J. Organomet. Chem.* **2005**, *690*, 2017–2026; b) N. Sedaghat, M. R. Naimi-Jamal, J. Mokhtari, *Curr. Chem. Lett.* **2014**, *3*, 57–62.
[19] Z. Otwinowski, W. Minor in *Methods in Enzymology*, vol. 276 ("Macrmolecular Crystallography Part A") (Eds.: C. W. Carter Jr., R. M. Sweet), Academic Press, New York, **1997**, pp. 307–326.
[20] *APEX2: Programs for data collection and data reduction*, Bruker-Nonius, Madison, **2012**.
[21] L. Krause, R. Herbst-Irmer, G. M. Sheldrick, D. Stalke, *J. Appl. Crystallogr.* **2015**, *48*, 3–10.
[22] S. Parkin, B. Moezzi, H. Hope, *J. Appl. Crystallogr.* **1995**, *28*, 53–56.
[23] G. M. Sheldrick, *Acta Crystallogr., Sect. A: Found. Crystallogr.* **2015**, *71*, 3–8.
[24] G. M. Sheldrick, *Acta Crystallogr., Sect. C: Struct. Chem.* **2015**, *71*, 3–8.
[25] P. van der Sluis, A. L. Spek, *Acta Crystallogr., Sect. A: Found. Crystallogr.* **1990**, *46*, 194–201.
[26] A. L. Spek, *Acta Crystallogr., Sect. D: Biol. Crystallogr.* **2009**, *65*, 148–155.
[27] S. Parkin, *Acta Crystallogr., Sect. A: Found. Crystallogr.* **2000**, *56*, 157–162.

Received: December 5, 2016